

RESEARCH

Open Access



# Investigation of Bursting Stress and Spalling Stress in Post-tensioned Anchorage Zones

Linyun Zhou\*

## Abstract

Over the past decades, considerable efforts have been made to quantify the bursting forces in the post-tensioned anchorage zones based on the simplified model or fitting formulas, however reproducing the transverse stress distribution is still a challenging topic, which is also important to detail the reinforcing details in the anchorage zones, especially for cracking control. To address this issue, this paper is devoted to seeking an elasticity solution for transverse stresses in the anchorage zones, and providing a more rational equation for transverse distribution in anchorage zones. The sum function of normal stresses is employed to solve the stresses filed in the anchorage zones with concentric load and two eccentric loads. The bursting stresses in the concentric anchorage zones and spalling stresses in the eccentric anchorage zones are verified by the photoelastic tests. The transverse stresses along the symmetry axis of the eccentric anchorage zones can be handled as a concentric single anchorage zone with equivalent bearing plate width. Moreover, according to the concept of force stream tube, the profiles of isostatic line of compression (ILCs) are determined and validated, which confirms the existence of ILCs.

**Keywords:** prestressed concrete, anchorage zone, bursting stress, spalling stress, photoelastic test, isostatic line of compression

## 1 Introduction

The anchorage zone is defined as the portion of structure in which the concentrated post-tensioning forces are transferred from the anchorage device to the structure. In post-tensioned anchorage zones, the spread of the concentrated forces will produce transverse tensile stresses, usually referred to as bursting stresses, along the tendon path. The resultant of the bursting stresses is called bursting forces. Practically, both the bursting forces and the bursting stresses are used to detail the reinforcing details in the anchorage zone.

To date, a large number of studies of the prediction of bursting stresses and bursting forces in anchorage zone have been conducted, including linear elastic studies,

finite element analysis, experimental studies and the strut-and-tie models.

Based on the theory of elasticity, Guyon (1953) studied the behavior of a concentric load applied over a rectangular body, and then provided a formulation to determine the bursting stress distribution ahead of a concentric end anchor for different bearing plate ratios. This relation was very influential in the design of anchorage zones. Yettram and Robbins (1970, 1971) reported that the location of uniform stress and the effect of Poisson's ratio were insignificant to the stress distribution based on elastic finite element analysis. Moreover, the extension of bursting stresses of I-sections was further than in rectangular sections and the flanges played an important role in reducing the spalling stresses. Sanders and Breen (1997) conducted experimental studies of anchorage zones with 36 specimens tested. By assuming that the resulting force at the end of the specimen would be shifted in the direction of the crack, the dispersion angle of the compressive strut should be reduced, then a modified

\*Correspondence: 101300072@seu.edu.cn

School of Transportation, Southeast University, Sipailou 2, Xuanwu district, Nanjing 210096, People's Republic of China  
Journal information: ISSN 1976-0485/eISSN 2234-1315

strut-and-tie model was proposed to predict the ultimate load of the anchorage zones. Wollmann (1991) conducted three experimental tests of concentric anchorage zones to study the influence of reaction forces on bursting stresses. For small tendon eccentricity, the influence of reaction forces on linear-elastic bursting forces and the resulting bursting force is conservative and can be neglected. Besides, the reaction forces have little influence on the failure mode of anchorage zones. Based on the results of those tests and finite element analyses, a fitting formula was proposed for calculating the bursting forces for typical anchorage zones (Breen et al., 1994), which had been adopted in the AASHTO-LRFD Bridge Design Specifications (2014) since 1994. Foster and Rogowsky (1997) studied the bursting stress distributions in the case of service load behavior, and distributions in the case of ultimate load behavior of anchorage zones by using rotating crack finite element model. They stated that the bursting stress distribution was flatter than that of the linear analysis due to the stress redistribution after cracking, which led to a conservative estimation of the bursting forces, and then a modified equation was proposed to estimate the load capacity of the anchorage zones. After analyzing the stress magnitudes and distributions of rectangular post-tensioned anchorage zones using ultra-high performance concrete (UHPC), Kim and Kim (2017) concluded that the use of UHPC gives significant reduction of anchorage zone size and no reinforcements are required. Yun (2005) proposed the nonlinear strut-and-tie model approach to predict the behavior of structural concrete, and then extended this study to the ultimate strengths of post-tensioned anchorages by checking the occurrence of a nodal zone failure mechanism, geometric compatibility condition, and the structural instability of the model struts and ties. Following the concept of isostatic line of compression (ILCs) initiated by Guyon (1953), Sahoo et al. (2009) presented an analytical equation for estimating the bursting stress and bursting forces by introducing certain boundary conditions of ILCs. However, this model was imperfect due to some questionable assumptions on the boundary conditions (Windisch, 2010). He and Liu (2011) proposed the compression dispersion model (CDM) by excluding the unreasonable assumptions in Sahoo's model. Nevertheless, the CDM failed to reproduce the bursting stresses along the tendon path due to insufficient boundary conditions. Based on the equilibrium condition at the far-end of the anchorage zones, Zhou et al. (2015) updated the CDM by incorporating two more boundary conditions, and verified by finite element analysis. However, in this updated model, the location of interface section of compressive and tensile stress was assumed to be constant, what is in contradiction with reality.

Over the past decades, considerable efforts have been made to quantify the bursting forces in the post-tensioned anchorage zones based on the simplified model or fitting formulas, however reproducing the transverse stress distribution is still a challenging topic, which is also important to detail the reinforcing details in the anchorage zone. To address this issue, this paper is devoted to seeking an analytical solution for transverse stresses in the anchorage zones, and providing a more rational equation for transverse distribution in anchorage zones.

## 2 Stress Solution of Anchorage Zones

### 2.1 Sum Function Method

According to the theory of elasticity (Timoshenko & Goodier, 1951), the equilibrium equation of the plane stress problem can be presented by

$$\frac{\partial \sigma_x}{\partial x} + \frac{\partial \tau_{xy}}{\partial y} = 0, \quad (1a)$$

$$\frac{\partial \sigma_y}{\partial y} + \frac{\partial \tau_{xy}}{\partial x} = 0, \quad (1b)$$

and then, the equilibrium differential equation can be given by

$$\nabla^2 \tau_{xy} = -\frac{\partial^2 I}{\partial x \partial y}, \quad (2)$$

in which  $\nabla^2 = \frac{\partial^2}{\partial x^2} + \frac{\partial^2}{\partial y^2}$ ;  $I = \sigma_x + \sigma_y$  is the sum function of normal stresses.

The stress solution should satisfy the harmonious equation, that is

$$\nabla^2 I = 0. \quad (3)$$

As can be seen, the sum function,  $I$ , can be figured out from harmonious equation; and then the shear stress can be obtained by substituting  $I$  into Eq. (2); finally, the stress components will be solved based on the equilibrium equations and boundary conditions.

### 2.2 Solution of Stress Components

For the problem as illustrated in Fig. 1, prescribed forces,  $q(y)$ , are symmetrically loaded on the plate. According to symmetries, the sum function,  $I$ , can be assumed as

$$I = \sum f(x) \cos \beta y, \quad (4)$$

in which  $\beta = n\pi/h$ ,  $f(x)$  is the undetermined functions, and  $h$  is the height of the plate.

Substituting Eq. (4) into Eq. (3) yields

$$\sum [f''(x) - \beta^2 f(x)] \cos \beta y = 0. \quad (5)$$

Then, the sum function,  $I$ , can be solved by

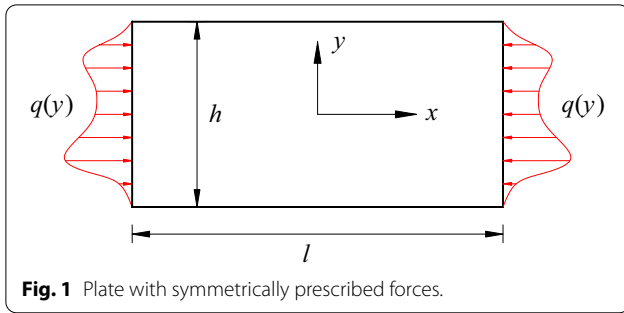


Fig. 1 Plate with symmetrically prescribed forces.

$$I = \sum (a_n ch\beta x + b_n sh\beta x) \cos \beta y, \tag{6}$$

in which coefficients  $a_n$  and  $b_n$  can be determined by boundary conditions.

Substituting sum function into Eq. (2), the shear stress can be derived by

$$\begin{aligned} \tau_{xy} = & \sum (c_n ch\beta x + d_n sh\beta x + \frac{a_n}{2} \beta x ch\beta x \\ & + \frac{b_n}{2} \beta x sh\beta x) \sin \beta y, \end{aligned}$$

where  $c_n$  and  $d_n$  are constraints determined by boundary conditions.

According to the relationship of normal stress and shear stress illustrated in equilibrium equation, we have

$$\begin{aligned} \frac{\partial \sigma_x}{\partial x} = & -\frac{\partial \tau_{xy}}{\partial y} \\ = & -\sum \beta (c_n ch\beta x + d_n sh\beta x + \frac{a_n}{2} \beta x ch\beta x \\ & + \frac{b_n}{2} \beta x sh\beta x) \cos \beta y, \end{aligned} \tag{8a}$$

$$\begin{aligned} \frac{\partial \sigma_y}{\partial y} = & -\frac{\partial \tau_{xy}}{\partial x} = -\sum \beta (c_n sh\beta x + d_n ch\beta x + \frac{a_n}{2} ch\beta x + \frac{b_n}{2} \beta sh\beta x \\ & + \frac{a_n}{2} \beta x sh\beta x + \frac{b_n}{2} \beta x ch\beta x) \sin \beta y. \end{aligned} \tag{8b}$$

Finally, the stress components can be derived by integrating the above equations:

$$\begin{aligned} \sigma_x = & -\sum (c_n sh\beta x + d_n ch\beta x + \frac{a_n}{2} \beta x sh\beta x \\ & - \frac{a_n}{2} ch\beta x + \frac{b_n}{2} \beta x ch\beta x \\ & - \frac{b_n}{2} sh\beta x) \cos \beta y + D_1(y), \end{aligned} \tag{9a}$$

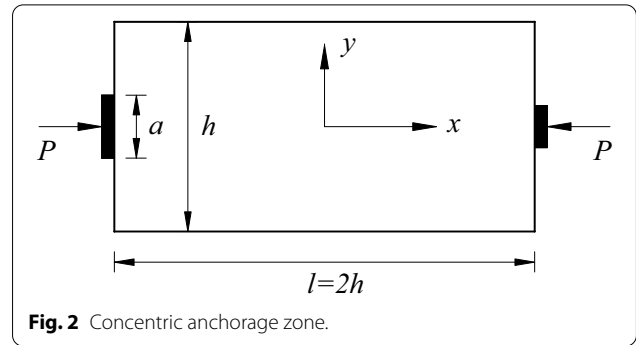


Fig. 2 Concentric anchorage zone.

$$\begin{aligned} \sigma_y = & \sum (c_n sh\beta x + d_n ch\beta x + \frac{a_n}{2} ch\beta x \\ & + \frac{a_n}{2} \beta x sh\beta x + \frac{b_n}{2} \beta x ch\beta x \\ & + \frac{b_n}{2} sh\beta x) \cos \beta y + D_2(x), \end{aligned} \tag{9b}$$

$$\tau_{xy} = \sum (c_n ch\beta x + d_n sh\beta x + \frac{a_n}{2} \beta x ch\beta x + \frac{b_n}{2} \beta x sh\beta x) \sin \beta y, \tag{9c}$$

in which function  $D_1(y)$  and  $D_2(x)$  are determined by the stress boundary conditions.

### 2.3 Transverse Stress in Concentric Single Anchorage Zone

According to Huang (2012), the anchorage shape and duct hole have little effect on bursting stresses and bursting forces, thus the concentric anchorage zone can be modeled as a plane stress problem as depicted in Fig. 2. The concentric anchor force,  $P$ , loaded on the bearing plate can be expressed by the Fourier series,

$$q(y) = A_0 - \sum A_n \cos \beta y, \tag{10}$$

in which

$$A_0 = \frac{aq}{h}, \tag{11a}$$

$$A_n = \frac{2q}{h\beta} \sin a\beta, \tag{11b}$$

where  $q = P/(at)$ ;  $a$  is the bearing plate width; and  $t$  is the thickness of the anchorage zone.

From the above equation, the anchor force can be treated as two parts, one of which is a uniform load,

$q_{11}(y) = A_0$ , and the other a polynomial distributed load,  $q_{12}(y) = \sum A_n \cos \beta y$ .

For the case of uniform load, the stress components in the anchorage zone can be given by

$$\sigma_x = -q_{11} = -aq/h, \tag{12a}$$

$$\sigma_y = 0, \tag{12b}$$

$$\tau_{xy} = 0. \tag{12c}$$

While for the case of distributed load, the stress boundary conditions can be presented by

$$\tau_{xy}|_{x=\pm l} = 0, \tag{13a}$$

$$\sigma_x|_{x=\pm l} = \sum A_n \cos \beta y, \tag{13b}$$

$$\int_{-l}^l \sigma_y dx = 0, \tag{13c}$$

$$\int_{-h}^h \sigma_x dy = P. \tag{13d}$$

Imposing the stress boundary equations into Eq. (9), we have

$$a_n = A_n \frac{2sh\beta l}{\beta l + sh\beta lch\beta l} \approx \frac{2A_n}{sh\beta l}, \tag{14a}$$

$$b_n = c_n = 0, \tag{14b}$$

$$d_n = -A_n \frac{\beta lch\beta l}{\beta l + sh\beta lch\beta l} \approx -\frac{A_n\beta l}{sh\beta l}, \tag{14c}$$

$$D_1(y) = D_2(x) = 0. \tag{14d}$$

Therefore, the stress induced by the distributed load can be presented by

$$\sigma_x = -\sum (d_nch\beta x + \frac{a_n}{2}\beta xsh\beta x - \frac{a_n}{2}ch\beta x) \cos \beta y, \tag{15a}$$

$$\sigma_y = \sum (d_nch\beta x + \frac{a_n}{2}ch\beta x + \frac{a_n}{2}\beta xsh\beta x) \cos \beta y, \tag{15b}$$

$$\tau_{xy} = \sum (d_nsh\beta x + \frac{a_n}{2}\beta xch\beta x) \sin \beta y. \tag{15c}$$

Finally, the stress components in the concentric anchorage zone can be derived by

$$\sigma_x = -\frac{aq}{h} - \sum (d_nch\beta x + \frac{a_n}{2}\beta xsh\beta x - \frac{a_n}{2}ch\beta x) \cos \beta y, \tag{16a}$$

$$\sigma_y = \sum (d_nch\beta x + \frac{a_n}{2}ch\beta x + \frac{a_n}{2}\beta xsh\beta x) \cos \beta y, \tag{16b}$$

$$\tau_{xy} = \sum (d_nsh\beta x + \frac{a_n}{2}\beta xch\beta x) \sin \beta y. \tag{16c}$$

According to Eq. (16b), the transverse stress along the tendon path, i.e.,  $y = 0$ , can be obtained by

$$\begin{aligned} \sigma_y &= \sum (d_nch\beta x + \frac{a_n}{2}ch\beta x + \frac{a_n}{2}\beta xsh\beta x) \\ &\approx \sum \frac{a_n}{2} (1 + \beta x - \beta l)ch\beta x. \end{aligned} \tag{17}$$

Representing the above equation by the fourth-order Taylor series expansion, that is,

$$\sigma_y = \sum \frac{A_n}{sh2n\pi} (\frac{\pi x}{h} - 5.28)(1 + \frac{\pi^2 x^2}{2h^2} + \frac{\pi^4 x^4}{24h^4}). \tag{18}$$

Cartesian coordinate system is established in the anchorage zone as shown in Fig. 3, the direction parallel to the load is set to be the x-axis. Therefore, the bursting stress in the concentric anchorage zone can be approximated by the first two terms:

$$\begin{aligned} \sigma_{Tc} &= -\frac{12P\sqrt{\sin(\pi a/2h)}(h-a)}{h^6 t} (x - \frac{h\sqrt{\sin(\pi a/2h)}}{4}) \\ &\quad (x-h)^3. \end{aligned} \tag{19}$$

It can be seen that the interface section of compressive and tensile stress is located at  $x_0 = \frac{h\sqrt{\sin(\pi a/2h)}}{6}$ , where the transverse stress is equal to zero. And the transverse stress reaches its maximum value  $\sigma_{Tc,max}$  at  $x = (h + 3x_0)/4$

$$\sigma_{Tc,max} \approx \frac{0.57P(h-a)}{h^2 t}. \tag{20}$$

Thus, the bursting force along the tendon axis  $T_b$  can be written as

$$T_b = \int_{x_0}^h \sigma_{Tc} t dx \approx 0.24P(1 - \frac{a}{h}). \tag{21}$$

It can be seen that the bursting forces in concentric anchorage zones agree well with the formulas given by current design codes (ACI 318-08 2008, AASHTO, 2014, CEB-FIP 1990)

$$T_b = 0.25P(1 - \frac{a}{h}). \tag{22}$$

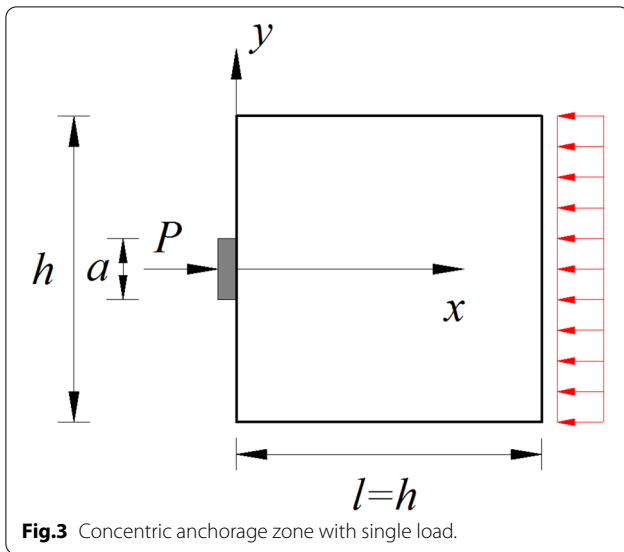


Fig. 3 Concentric anchorage zone with single load.

**2.4 Transverse Stress in Anchorage Zones with Two Anchors**

As for the problem illustrated in Fig. 4, the two anchor forces, having their centers at a distance  $e$  in the  $x$ -direction, can be expressed by

$$q(y) = B_0 + \sum B_n \cos \beta y, \tag{23a}$$

in which

$$B_0 = \frac{2aq}{h}, \tag{23b}$$

$$B_n = \frac{4q}{\beta h} \cos e\beta \sin a\beta. \tag{23c}$$

Similarly, the anchor forces can be divided into two parts, that is, a uniform load,  $q_{21}(y) = B_0$ , and a polynomial distributed load,  $q_{22}(y) = \sum B_n \cos \beta y$ .

Following the similar method as mentioned before, the stress solution of the anchorage zone with two eccentric anchor loads can be given by

$$\sigma_x = -\frac{2aq}{h} - \sum (d_n ch\beta x + \frac{a_n}{2} \beta x sh\beta x - \frac{a_n}{2} ch\beta x) \cos \beta y, \tag{24a}$$

$$\sigma_y = \sum (d_n ch\beta x + \frac{a_n}{2} ch\beta x + \frac{a_n}{2} \beta x sh\beta x) \cos \beta y, \tag{24b}$$

$$\tau_{xy} = \sum (d_n sh\beta x + \frac{a_n}{2} \beta x ch\beta x) \sin \beta y, \tag{24c}$$

in which

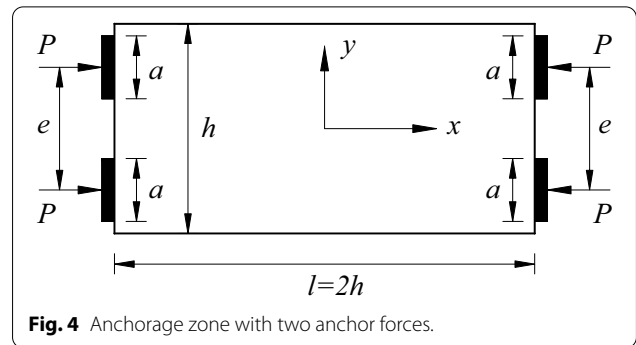


Fig. 4 Anchorage zone with two anchor forces.

$$a_n = B_n \frac{2sh\beta l}{\beta l + sh\beta lch\beta l} \approx \frac{2B_n}{sh\beta l}, \tag{25a}$$

$$d_n = -B_n \frac{\beta lch\beta l}{\beta l + sh\beta lch\beta l} \approx -\frac{B_n \beta l}{sh\beta l}. \tag{25b}$$

Then, the transverse stress,  $\sigma_y$ , in the Cartesian coordinate system as shown in Fig. 5, can be approximated by

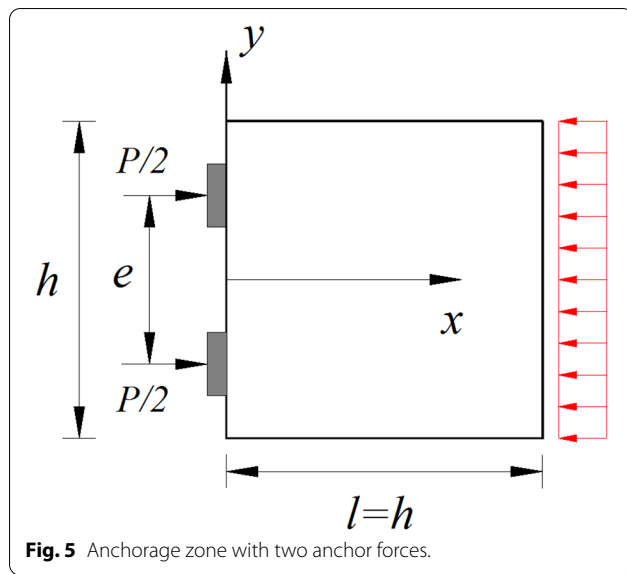
$$\sigma_y \approx \frac{4q}{\pi sh 2\pi} \cos \frac{e\pi}{h} \sin \frac{a\pi}{h} (1 + \frac{\pi}{h} x) ch(\frac{\pi}{h} x - 2\pi) \cos \frac{\pi}{h} y. \tag{26}$$

As can be seen, the magnitude of transverse stress is mainly dependent on the eccentricity  $e$ . When the anchor devices are placed at the quarter points, that is  $e = h/2$ , no transverse stress will be produced in the anchorage zone. While for the case of the anchor forces acting over half of the depth, that is,  $e > h/2$ , strain compatibility will produce spalling stress between the anchors, and the dispersion of concentric loads will generate bursting stress. Similarly, the spalling stress along the  $x$ -axis,  $\sigma_{Ts}$ , and the transverse bursting stress along the tendon path,  $\sigma_{Tb}$ , can be approximated by

$$\sigma_{Ts} = \frac{26P \sqrt{\sin \pi a_s / 2h} (h - a_s)}{h^6 t} \left[ x - \frac{h \sqrt{\sin \pi a_s / 2h}}{6} \right] (x - h)^3, \tag{27a}$$

$$\sigma_{Tb} = -\frac{6P \sqrt{\sin \pi a / 2h'} (h' - a)}{h'^6 t} \left[ x - \frac{h' \sqrt{\sin \pi a / 2h'}}{6} \right] (x - h')^3, \tag{27b}$$

in which  $a_s = 2e - h$ ; and  $h' = h - e$ .



Equation (27) shows that the bursting stress along the tendon path in the anchorage zone with two eccentric anchor loads is equal to the bursting stress in the concentric anchorage zone with the depth  $h' = h - e$ , which is the principle of symmetrical prism proposed by Guyon (1953).

The corresponding spalling forces,  $T_s$ , and bursting forces,  $T_b$ , can be given by

$$T_s \approx 0.12 \frac{P(h - a_s)}{h}, \tag{28a}$$

$$T_b \approx 0.12P \left(1 - \frac{a}{h - e}\right). \tag{28b}$$

While for the case of  $e < h/2$ , the transverse stress along the  $x$ -axis,  $\sigma_{Tb}$ , can be rearranged by

$$\sigma_T = - \frac{12P \sqrt{\sin \pi a_b / 2h} (h - a_b)}{h^6 t} \left[ x - \frac{h \sqrt{\sin \pi a_b / 2h}}{6} \right] (x - h)^3, \tag{29}$$

where  $a_b = 2e$ .

Then, the bursting forces,  $T_b$ , can be obtained by

$$T_b \approx 0.24P \left(1 - \frac{e}{h}\right). \tag{30}$$

It can be seen that when the multi-anchors are placed inside the quarter points, that is, the anchor spacing is less than  $0.5h$ , the multi anchorage zone can be handled as a concentric anchorage zone with the bearing plate width  $a_b = 2e$ ; while the two anchors are placed outside

the quarter points, the spalling stress will be produced between the anchors, and its distribution can be approximated by the negative value of the bursting stress in the concentric anchorage zone with bearing plate width  $a_s = 2e - h$ . Thus, a unified equation can be presented to express the transverse stress along the centerline of anchorage zone

$$\sigma_{Tb} = \mp \frac{12P \sqrt{\sin \pi a_e / 2h} (h - a_e)}{h^6 t} \left[ x - \frac{h \sqrt{\sin \pi a_e / 2h}}{6} \right] (x - h)^3, \tag{31}$$

in which  $a_e$  is the equivalent bearing plate width and can be defined by

$$a_e = \begin{cases} e & e < h/2 \\ e - h/2 & e > h/2 \end{cases}. \tag{32}$$

### 3 Validation

#### 3.1 Test Program

In order to verify the accuracy of the proposed equations, 10 photoelastic tests (Timoshenko & Goodier, 1951) have been carried out. All the test specimens are made of polycarbonate, and have the rectangular cross section  $b \times t = 80 \times 8 \text{ mm}$ . Young's modulus of polycarbonate is taken to be  $E = 3200 \text{ MPa}$ , Poisson's ratio as  $\nu = 0.37$ , and photoelastic material fringe value as  $f = 308 \text{ N/order/m}$ . Details of the test specimens are listed in Table 1. All of the test specimens are monotonically loaded over the full thickness so that the specimen would behave as two-dimensional as possible. Specimens C1–C5 were tested to investigate the effect of the bearing plate ratio to the transverse bursting stress in concentric anchorage zones as shown in Fig. 6; while M1–M5 were tested to study the influence of eccentricities on transverse stress.

Fig. 7 illustrates the experimental setup to obtain photoelasticity images, which consists of light source, polarizer, quarter wave plate, analyzer and camera. Two setups were used, one for employing white light and the other for monochromatic light, the use of which will be explained later.

#### 3.2 Test Procedure

During the test, the light will be linearly polarized by the polarizer and circularly polarized by the first quarter wave plate. After passing through the test specimen, the light is linearly polarized by the second quarter wave plate and passes through the analyzer, which creates dark or bright regions, i.e., the fringe pattern. The

**Table 1** Details of the test specimens.

Specimen	height $h$ (mm)	Bearing plate ratio $a/h$	Anchor spacing $e/h$	Applied load $P$ (N)
C1	80	0.1	0	33
C2	80	0.2	0	58
C3	80	0.3	0	60
C4	80	0.4	0	60
C5	80	0.5	0	66
M1	80	0.1	0.3	32
M2	80	0.1	0.4	38
M3	80	0.1	0.5	40
M4	80	0.1	0.6	40
M5	80	0.1	0.8	40

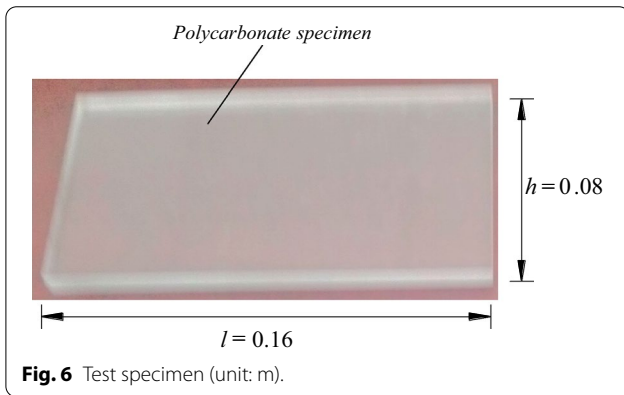


**Fig. 6** Test specimen (unit: m).

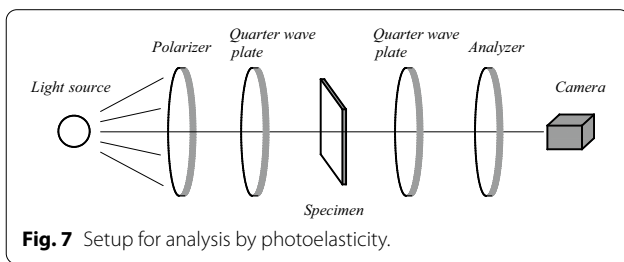


**Fig. 7** Setup for analysis by photoelasticity.

fringe pattern is then captured by the camera. The brief test can be illustrated as following:

1. Apply load gradually to the test specimen in the circular polariscope system obtained from the white light source. Capture the isochromatic patterns (see Figs. 8a and 9a).
2. In the dark-field orthogonal linear polarization system obtained from the monochromatic light, make sure that the polarization axis of the polarizer is par-

allel to the ground and that of the analyzer is vertical to the ground. Capture the isoclines patterns.

3. Rotate polarizer and analyzer by 5 degrees simultaneously. Capture the isoclines patterns.
4. Repeat step 3 until the a complete rotation of 90 degrees. Capture the isoclines patterns (see Figs. 8b and 9b).

### 3.3 Stress Solution

According to the photoelasticity images captured by camera, the isochromatic and isocline patterns can be sketched as shown in Fig. 10a. Following the shear difference method (Frocht 1941), the stress components in the desired integration path  $MN$  (see Fig. 10b) can be given by

$$(\sigma_x)_i = (\sigma_x)_{i-1} - (\Delta\tau_{xy})_{i-1}^i \frac{\Delta x}{\Delta y}, \tag{33a}$$

$$(\sigma_y)_i = (\sigma_x)_i \pm |m \cos 2\alpha|, \tag{33b}$$

$$\tau_{xy} = \frac{m}{2} \sin 2\alpha, \tag{33c}$$

in which

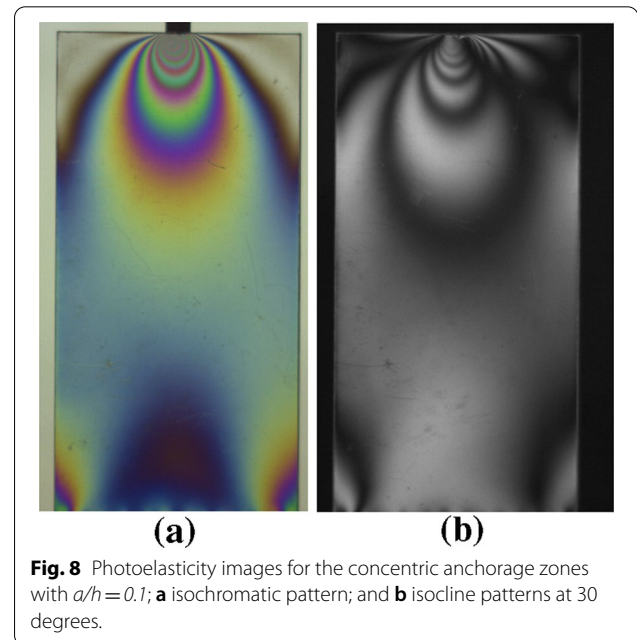
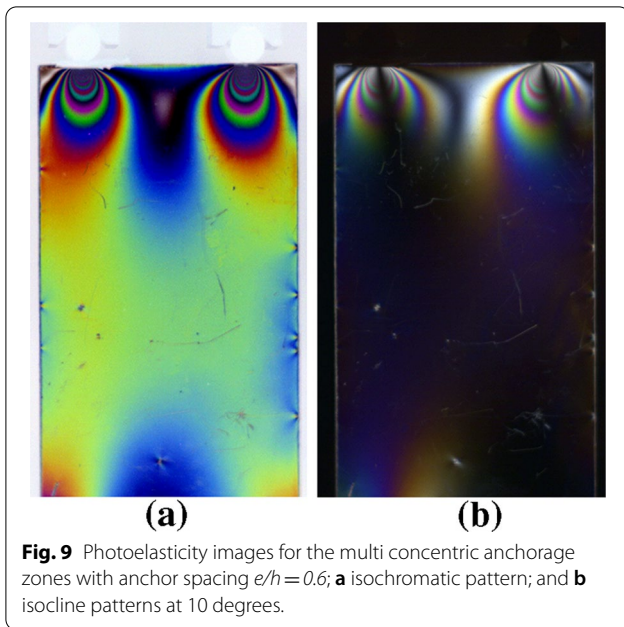


**Fig. 8** Photoelasticity images for the concentric anchorage zones with  $a/h = 0.1$ ; **a** isochromatic pattern; and **b** isocline patterns at 30 degrees.



$$\Delta\tau_{xy} = (\tau_{xy})_{AB} - (\tau_{xy})_{CD}, \tag{34a}$$

$$(\Delta\tau_{xy})_{i-1}^i = \frac{(\Delta\tau_{xy})_{i-1} + (\Delta\tau_{xy})_i}{2}, \tag{34b}$$

where  $m$  is the order isochromatic,  $\alpha$  is the inclination of the isocline with respect to  $x$ -axis.

Table 2 lists the stress solution of the section  $MN$ , at a depth of  $0.5 h$  below the loading plate, in the concentric anchorage zone with  $a/h = 0.1$ . Fig. 11a, b show the test normal stress components in anchorage zone with single concentric load and two eccentric anchor loads.

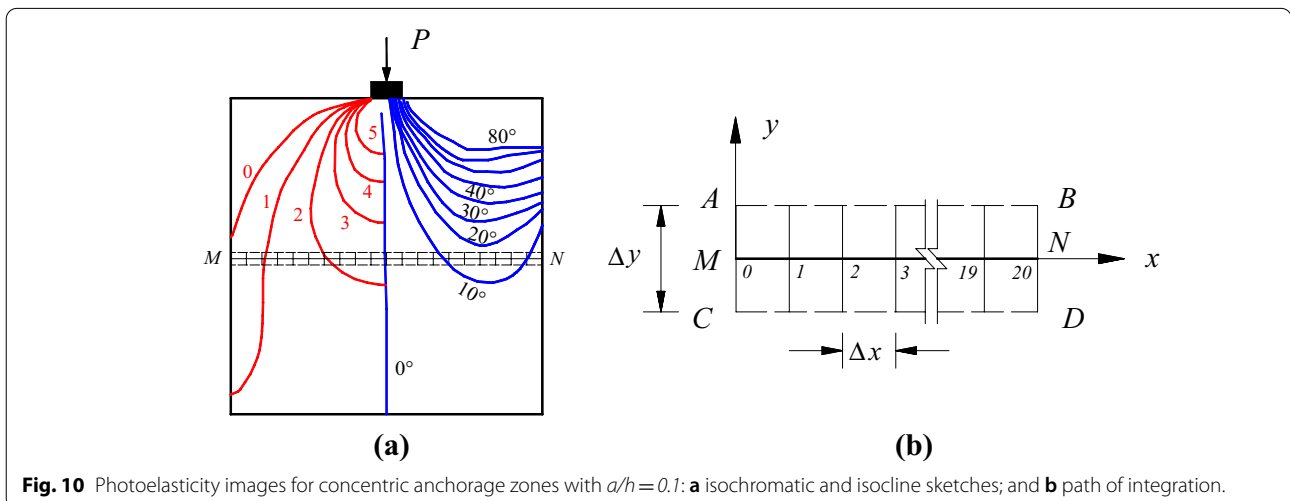
### 3.4 Concentric Anchorage Zones

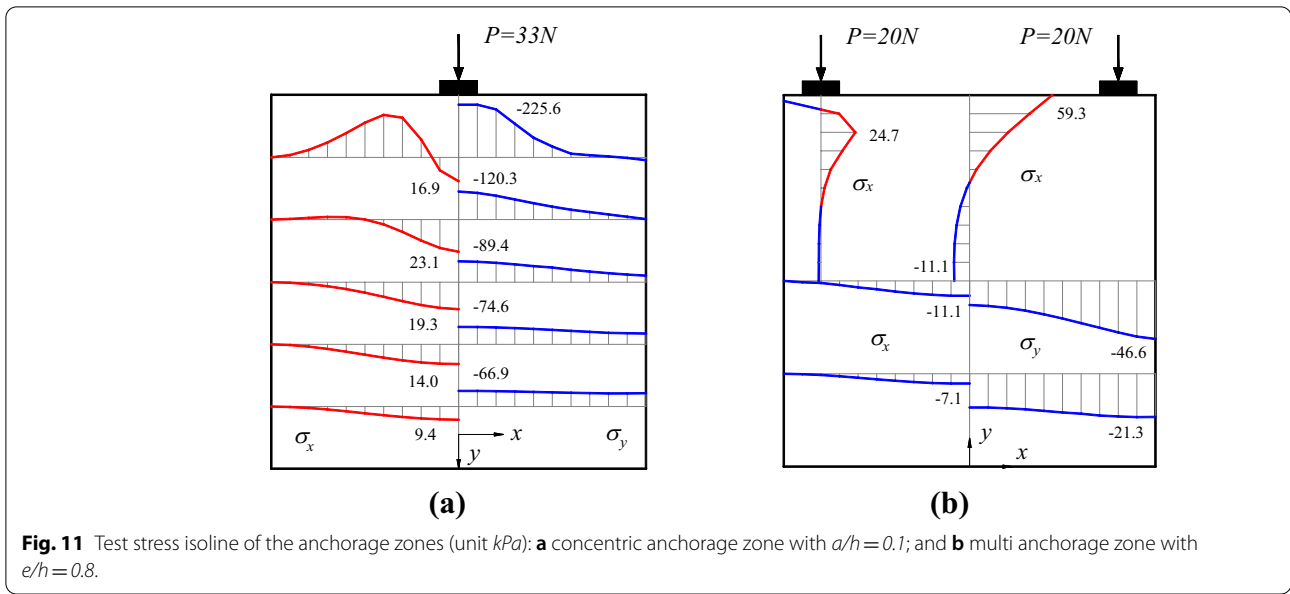
Fig. 12 shows the comparisons of the bursting stresses in the concentric anchorage zones calculated by different methods. It can be seen that the proposed equation can predict the transverse tensile stress accurately, and the maximum relative error is only 3.2%. It also should be noted that the interface section of compressive and tensile stress, where transverse stress  $\sigma_b = 0$ , varies with the bearing plate ratio. In recent previous analytical studies of the bursting stresses (He et al., 2011; Zhou et al., 2015), the interface section was assumed to be constant. Actually, as early as 1950s, Guyon (1953) presented a fitting formula to capture the location of this section as shown in Fig. 13. It is clear that both Eq. (19) and Guyon’s formula (1953) produce a good agreement with the test results, and the predicted values of Eq. (19) are on average 96.4% of the test values, with a standard deviation of 2.7%; these two numbers are 104.8% and 3.7%, respectively, for Guyon equation (1953).

Fig. 14 illustrates the comparison of bursting force with different bearing plate ratios. As can be seen, both Eq. (21) and AASHTO (2014) equation agree well with the test results. The average relative deviations are only 5.7 and 3.8%, respectively.

### 3.5 Two Anchorage Zones

The transverse stress along the centerline of specimen for the anchorage zone with two eccentric anchor loads with different anchor spacing is illustrated in Fig. 15. It can be seen that the proposed Eq. (30) give very close results to the test transverse stress. The average relative deviation is only 4.8%. Fig. 16 shows the influence of the anchor spacing on the transverse tensile forces in anchorage zones (the size of anchor plate is kept constant at  $a = 0.1 h$ ). It





**Fig. 11** Test stress isoline of the anchorage zones (unit kPa): **a** concentric anchorage zone with  $a/h = 0.1$ ; and **b** multi anchorage zone with  $e/h = 0.8$ .

**Table 2** Stress components calculated by shear difference method.

Node	Section AB			Section CD			Section MN		
	$m$ (order)	$\alpha$ ( $^\circ$ )	$\tau_{AB}$ (kPa/order)	$m$ (order)	$\alpha$ ( $^\circ$ )	$\tau_{AB}$ (kPa/order)	$\sigma_x$ (kPa)	$\sigma_y$ (kPa)	$\tau_{xy}$ (kPa)
0	0.26	3.8	0.02	0.76	1.88	0.02	0.0	-24.1	0.0
1	0.58	10.9	0.11	0.88	8.0	0.12	0.3	-29.1	-0.2
2	0.92	16.5	0.25	1.12	9.9	0.19	1.2	-35.3	-0.6
3	1.38	16.7	0.38	1.75	12.9	0.38	2.3	-46.4	-1.3
4	1.61	16.7	0.44	1.83	14.2	0.43	4.2	-49.4	-2.1
5	1.78	15.3	0.45	2.01	12.2	0.41	6.9	-58.4	-2.7
6	1.98	13.7	0.45	2.24	9.8	0.37	9.2	-66.1	-3.2
7	2.28	10.2	0.40	2.49	7.4	0.32	12.3	-74.5	-3.3
8	2.51	7.2	0.31	2.66	4.6	0.21	15.8	-81.0	-2.7
9	2.69	4.1	0.19	2.75	3.2	0.15	18.4	-87.1	-1.6
10	2.76	0.0	0.00	2.83	0.0	0.00	19.0	-87.8	0.0

Note: the values are for "at the location of 0.5 h below the loading plate in the concentric anchorage zone with  $a/h = 0.1$ "

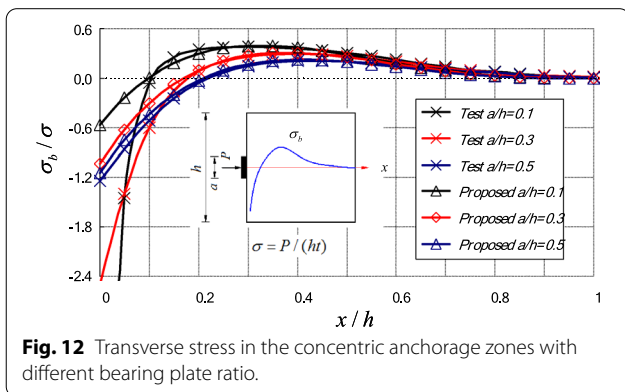


**Fig. 12** Transverse stress in the concentric anchorage zones with different bearing plate ratio.

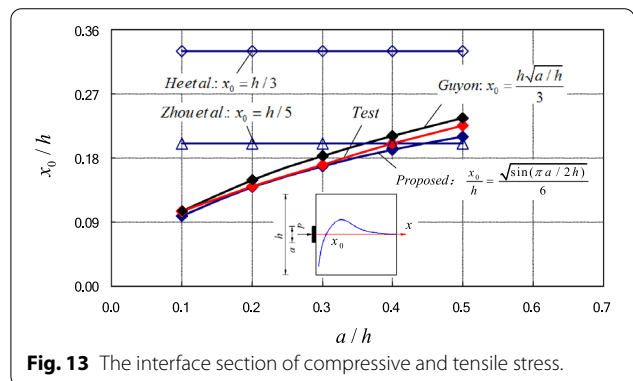


**Fig. 13** The interface section of compressive and tensile stress.

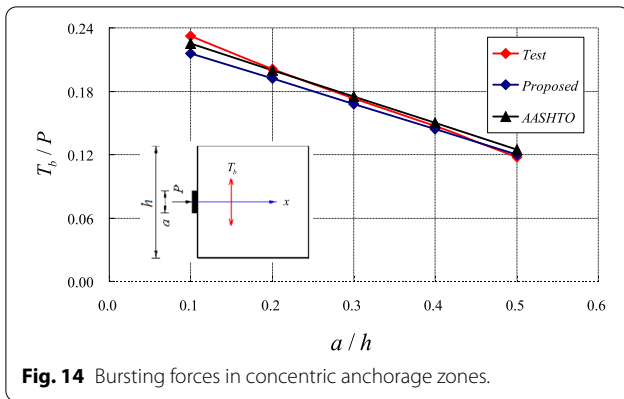


**Fig. 14** Bursting forces in concentric anchorage zones.

indicates that the proposed equation produces a good agreement with the test results, the average relative deviation is only 4.0%.

#### 4 Towards the Existence of ILCs

As early as 1953, Guyon (1953) used the ILCs to visualize the flow of forces in post-tensioned anchorage zones as shown in Fig. 17. Each individual ILC transfers an equal share of the force, which induces a certain amount of transverse stress depending on its curvature. However, this is just a conceptual model, and the existence of ILCs is presently unproven.

Although the longitudinal compressive stress in anchorage zones will be effected by the duct hole significantly (Park et al., 2020), it has little effect on the distribution of transverse bursting stress (Huang, 2012). Thus, the anchorage zone can be idealized as a concrete block without hole. According to the concept of Guyon

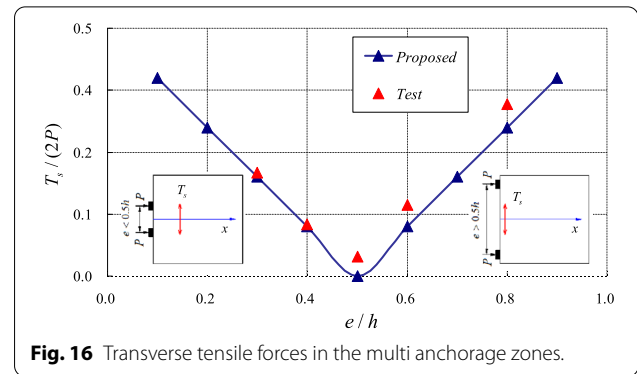


**Fig. 16** Transverse tensile forces in the multi anchorage zones.

(1953), there must exist an ILC along the centerline of the anchorage zone. Referring to Fig. 18a, the force stream tube (Kelly & Elsley, 1995) bounded by two ILCs is considered. The force over flow tube should satisfy

$$F_j = F_{j-1} = P\Delta a/a, \tag{35}$$

in which  $P$  is the anchor force; and  $a$  is width of anchorage zone;  $\Delta a$  is the vertical distance between the centerline line and ILC;  $F_j$  is the force in the stream tube in the arbitrary section and can be defined by

$$F_j = \frac{(\sigma_{x,Aj} + \sigma_{x,Bj})t}{2 \cos \frac{\theta_j}{2}} y_j, \tag{36}$$

in which  $\sigma_{y,Aj}$  and  $\sigma_{y,Bj}$  are the  $x$ -direction normal stresses of the centerline and ILC at  $x = A_j$ , respectively;  $t$  is the thickness of anchorage zone;  $y_j$  is the vertical distance between the centerline line and ILC at  $x = A_j$ ; and  $\theta_j$  is the local angular orientation of the force tube wall.

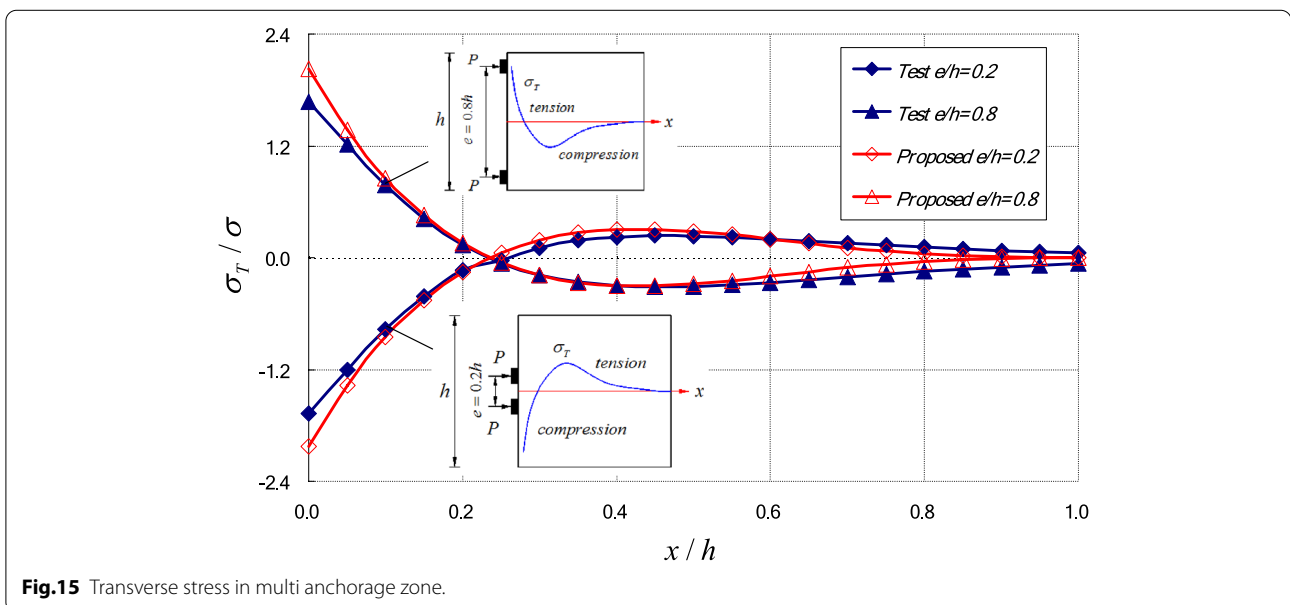


**Fig.15** Transverse stress in multi anchorage zone.

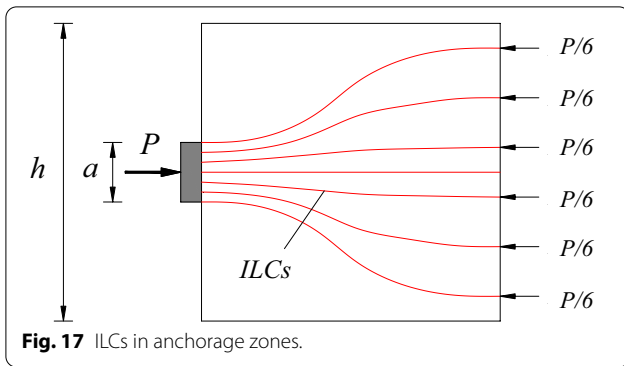


**Fig. 17** ILCs in anchorage zones.

Substituting Eq. (35) into Eq. (36) leads to

$$y_j = \frac{2P}{(\sigma_{x,A_j} + \sigma_{x,B_j})t} \frac{\Delta a}{a} \cos \frac{\theta_j}{2}. \tag{37}$$

According to the geometrical condition of the ILC as illustrated in Fig. 18b, we have

$$y_j = y_{j-1} + \Delta x \tan \theta_{j-1}. \tag{38}$$

As can be seen from the above equation, if  $y_1 = \Delta a$  and  $\Delta x$  is specified, the vertical location of the ILCs will be determined by an iterative solution. Fig. 19 illustrates the shapes of ILCs in concentric anchorage zone with different bearing plate ratios, in which only a single ILC is plotted for the sake of simplification.

Thus, the bursting forces can be derived by

$$T = \int \sigma_{trans} t dx = \int -\frac{P}{t} \frac{d^2 y}{dx^2} t dx = -P \frac{dy}{dx} \Big|_{x=x_0}. \tag{39}$$

According to the geometrical condition as shown in Fig. 19, the slope of the ILCs at the inflection point can be approximated by

$$\frac{dy}{dx} \Big|_{x=x_0} = \tan \theta \approx 2m/(1 - m^2), \tag{40}$$

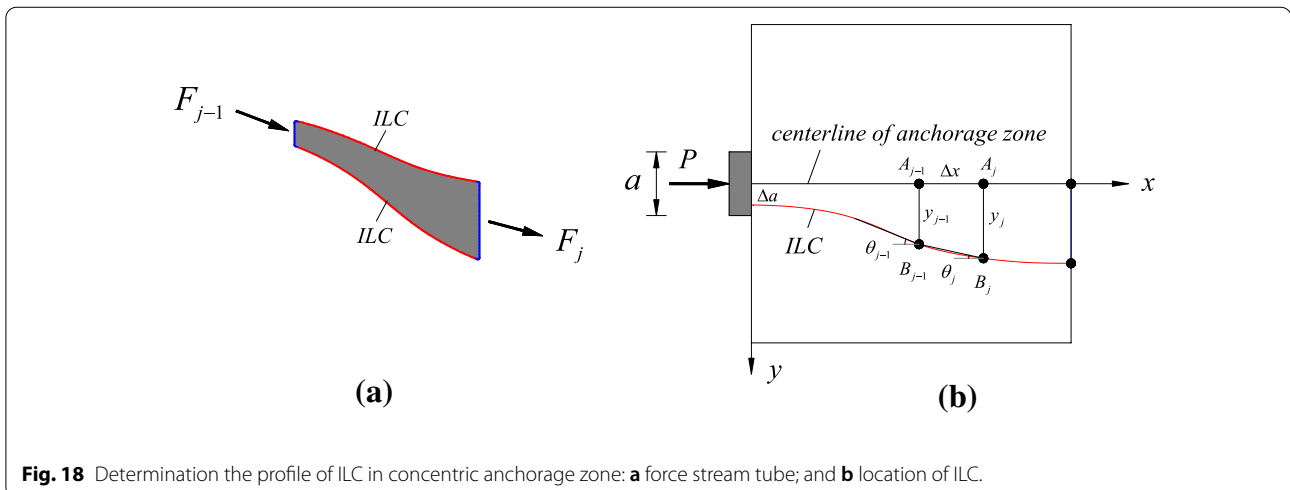
in which  $m = (\Delta h - \Delta a)/l$ ;  $\Delta h$  and  $\Delta a$  are the vertical value of ILCs at starting point and ending point, respectively.

Table 3 lists the bursting forces in the concentric anchorage zone predicted by the proposed equation and ILCs. As can be seen, the predictions of ILCs agree well with the test results. The average discrepancy between the ILCs predictions and test results is only 13%, which is mainly induced by iterative process. Therefore, the ILCs found by proposed method can reveal the load transfer mechanism in anchorage zones. That is, ILCs are real existence in the anchorage zones and transmit the anchor loads to the far-end section.

### 5 Conclusions

To clear the stress field in the anchorage zones, an elasticity solution of the transverse stress is derived based on the sum function method. The sum function of normal stresses can be figured out from harmonious equation, and then the stress field in the anchorage zone can be determined by equilibrium equations and boundary conditions. According to the photoelastic test results and their comparison with the proposed equations, the following conclusions can be drawn:

- (1) The proposed equations can reproduce the transverse stress in concentric anchorage zones, and is verified to have good accuracy by comparisons with test results. On the other hand, the other existing



**Fig. 18** Determination the profile of ILC in concentric anchorage zone: **a** force stream tube; and **b** location of ILC.

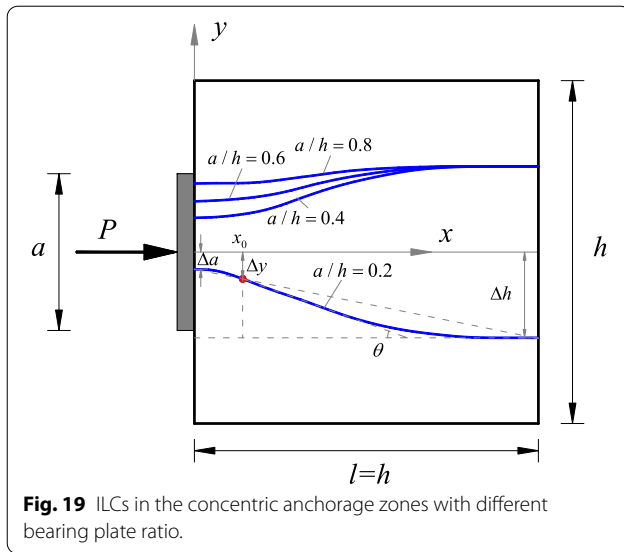


**Fig. 19** ILCs in the concentric anchorage zones with different bearing plate ratio.

analytical models cannot predict the transverse stress distribution accurately, due to the incorrect location of the interface section of compressive and tensile stress.

- (2) The transverse stress along the symmetry axis of the anchorage zone with two eccentric anchor loads can be handled as a concentric single anchorage zone with equivalent bearing plate width.
- (3) It is very interesting that the bursting stress along the tendon path in the anchorage zone with two anchors is equal to the bursting stress in the concentric anchorage zone with the depth  $h' = h - e$ , which is the principle of symmetrical prism.
- (4) The major significance of this investigation not only lies in reproducing the transverse stress in anchorage zones, but also in confirming the existence of the ILCs.

**Table 3** Bursting forces calculated by different methods.

$a/h$	$h$ (mm)	$m$	Bursting forces $T$		
			Test	Equation (21)/Test	ILCs/Test
0.1	0.08	0.104	0.23P	0.93	0.81
0.2	0.08	0.105	0.20P	0.96	0.84
0.3	0.08	0.106	0.17P	0.97	0.86
0.4	0.08	0.107	0.15P	0.98	0.89
0.5	0.08	0.109	0.12P	1.02	0.93
Mean				0.97	0.87
Standard deviation				0.03	0.05

**Abbreviations**

$a$ : Width of the bearing plate along the direction of the beam height;  $h$ : Height of the beam;  $t$ : Thickness of the anchorage zone;  $P$ : Anchor force;  $e$ : Eccentricity of the anchoring point to the centroid anchorage zone;  $\sigma_x, \sigma_y, \tau_{xy}$ : Normal stresses and shear stress;  $I = \sigma_x + \sigma_y$ : Sum function of normal stresses;  $\sigma_{T_c}$ : Bursting stresses distribution of concentric anchorage zone;  $\sigma_{T_{max}}$ : Maximum bursting stresses in concentric anchorage zone;  $T_b$ : Bursting force in concentric anchorage zone;  $\sigma_{T_e}$ : Bursting stresses distribution of eccentric anchorage zone;  $\sigma_{T_s}$ : Spalling stresses of eccentric anchorage zone;  $T_b$ : Bursting force in eccentric anchorage zone;  $T_s$ : Spalling force in eccentric anchorage zone;  $\sigma_T$ : Transverse stress along the centerline of anchorage zone;  $a_e$ : Equivalent bearing plate width;  $F_f$ : Force in stream tube at arbitrary section;  $y_j$ : Vertical distance between the centerline line and ILC;  $\theta_j$ : Local angular orientation of the force tube wall;  $\Delta h, \Delta a$ : Vertical value of ILCs at starting point and ending point, respectively.

**Acknowledgements**

The research team for new long-span bridges in Southeast University, Nanjing, China, is gratefully acknowledged for the test program in this paper.

**Authors' contributions**

The author has contributed substantially to all aspects of this article. The author read and approved the final manuscript, and has the appropriate permission and rights to the reported data. All authors read and approved the final manuscript.

**Authors' information**

Linyun Zhou is a post-doc in Southeast University, School of Transportation. His research interest included strut-and-tie model, bridge engineering, and UHPC.

**Funding**

This study was supported by the National Natural Science Foundation of China (Grant No. 51808208) and the fundamental research funds for the central universities (Grant No. 2242021R20011).

**Availability of data and materials**

All data, models, or code that support the findings of this study are available from the corresponding author upon reasonable request. All data, models, and code generated or used during the study appear in the submitted article.

**Declarations**

**Competing interests**

The authors declare that there have no competing interests in this paper.

Received: 13 March 2021 Accepted: 9 December 2021

Published online: 23 December 2021

**References**

AASHTO. (2014). *AASHTO LRFD bridge design specifications*. American Association of State Highway and Transportation Officials.

ACI committee 318, (2008). *Building Code Requirements for Structural Concrete (ACI 318-08) and Commentary (ACI 318R-08)*. Farmington Hills (MI), American Concrete Institute.

Breen, J. E., Burdet, O., Roberts, C., Sanders, D., & Wollmann G. (1994). Anchorage zone reinforcement for post-tensioned concrete girders, National Cooperative Highway Research Program Report 356, Washington, D. C., p. 8–11.

Comité Euro-International du Béton, Fédération International de la Précontrainte (CEB-FIP), (1990). *Practical design of structural concrete*. London, UK.

Foster, J., & Rogowsky, M. (1997). Bursting forces in concrete panels resulting from in-plane concentrated loads. *Magazine of Concrete Research*, 180, 231–240.

Frocht, M.M. (1941). Photoelasticity. John Wiley & Sons, Inc.

Guyon, Y. (1953). *Prestressed concrete*. John Wiley and Sons Inc.

- He, Z., & Liu, Z. (2011). Investigation of bursting forces in anchorage zones: Compression-dispersion models and unified design equation. *ASCE Journal of Bridge Engineering*, 16(6), 820–827.
- Huang, H. Q. (2012). *Reinforcement design for anchorage zone in post tensioned end block based on strut and tie model*. Master thesis, Southeast University.
- Kelly, D., & Elsley, A. (1995). Procedure for determining load paths in elastic continua. *Engineering Computations*, 5, 415–424.
- Kim, J. S., & Kim, T. H. (2017). A stress analysis of the post-tensioned anchorage zones using UHPC. *Key Engineering Materials*, 737, 500–504.
- Park, Y. H., Kim, M. Y., Park, J. M., & Jeon, S. J. (2020). An improved equation for predicting compressive stress in posttensioned anchorage zone. *Advances in Civil Engineering*, 2020, 5635060.
- Sahoo, D. K., Singh, B., & Bhargava, P. (2009). Investigation of dispersion of compression in bottle-shaped struts. *ACI Structural Journal*, 106, 178–186.
- Sanders, D., & Breen, J. E. (1997). Post-tensioned anchorage zones with single straight concentric anchorages. *ACI Structural Journal*, 2, 146–158.
- Timoshenko, S., & Goodier, J. (1951). *Theory of elasticity*. McGraw-Hill book company.
- Windisch, A. (2010). Investigation of dispersion of compression in bottle-shaped struts-discussion. *ACI Structural Journal*, 107, 124–126.
- Wollmann, G. (1991). *Design of anchorage zones in post-tensioned concrete structures*. PhD dissertation, University of Texas at Austin.
- Yettram, A. L., & Robbins, K. (1970). Anchorage zone stresses in post-tensioned uniform members with eccentric and multiple anchorages. *Magazine of Concrete Research*, 73, 209–218.
- Yettram, A. L., & Robbins, K. (1971). Anchorage zone stresses in axially post-tensioned I-section members with end-blocks. *Magazine of Concrete Research*, 74, 37–42.
- Yun, Y. M. (2005). Evaluation of ultimate strength of post-tensioned anchorage zones. *Journal of Advanced Concrete Technology*, 3, 149–159.
- Zhou, L., Liu, Z., & He, Z. (2015). Further investigation of transverse stresses and bursting forces in post-tensioned anchorage zones. *Structural Concrete*, 16, 84–92.

## Publisher's Note

Springer Nature remains neutral with regard to jurisdictional claims in published maps and institutional affiliations.

Submit your manuscript to a SpringerOpen<sup>®</sup> journal and benefit from:

- ▶ Convenient online submission
- ▶ Rigorous peer review
- ▶ Open access: articles freely available online
- ▶ High visibility within the field
- ▶ Retaining the copyright to your article

---

Submit your next manuscript at ▶ [springeropen.com](https://www.springeropen.com)

---